

Electrochemical Performances of Tin Oxide-Mesoporous Carbon Composites for Lithium Ion Battery Application

Hang T. T. Le^{1*}, Yen Thi Nguyen², Dang Viet Anh Dung¹, Chan-Jin Park³

¹ Hanoi University of Science and Technology, No. 1, Dai Co Viet, Hai Ba Trung, Ha Noi, Viet Nam

² Vietnam-Russia Tropical center, Institute of Tropical Durability, No. 63 Nguyen Van Huyen, Hanoi, Vietnam

³ Chonnam National University, 77, Yongbongro, Bukgu, Gwangju, South Korea

Received: november 26, 2018; Accepted: June 24, 2019

Abstract

A composite of tin oxide (SnO_2) and mesoporous carbon (namely HCMK3) was synthesized and investigated as anode active material for rechargeable lithium ion batteries. Nanostructured composite was prepared by incipient wetness impregnation technique in combination with a chemical reduction method. The resultant composite was 800 nm-nanorods, which were composed of discrete SnO_2 nanocrystals with a size of about 3 nm filling both inside and outside the mesopores of HCMK3 carbon. The obtained electrochemical results demonstrated that owing to its novel architecture, the composite electrode showed outstanding reversible capacity, excellent rate capability, and superior long-term cycling performance. Even at a high charge-discharge rate of 1C, a high reversible capacity of 398.6 mAh g^{-1} was achieved after 500 cycles.

Keywords: HCMK3, mesoporous carbon, composites, lithium ion batteries

1. Introduction

Recently, tin dioxide (SnO_2) has received considerable attentions as promising alternative candidate for commercial graphite anode in lithium ion batteries (LIBs) owing to its high theoretical capacity of 1494 mAh g^{-1} (based on insertion/conversion/alloy reaction), simple processing, low cost, earth abundance and low toxicity. Additionally, the lithiation/delithiation process of alloying reaction of this material occurs at the moderate plateau voltage of ~ 0.5 V vs. Li^+/Li , thus posing less safety issues. To date, numerous nanostructures of SnO_2 have been developed and show remarkable improvement in their electrochemical behaviour [1-4]. Unfortunately, SnO_2 suffers a severe volume change (over 300 %) during charge/discharge process. This leads to pulverization of the electrode active materials, loss of electrical contact between the active materials and the current collector, and deterioration of the solid electrolyte interphase (SEI) layer [5]. Thereby, to maintain the structural integrity for SnO_2 , buffer materials should be introduced. Among the buffer materials, carbon has been considered as a reasonable candidate due to its good lithium intercalation and de-intercalation reversibility [6]. In combination with SnO_2 carbon not only works as electrode active material but also play a role of buffer layer for SnO_2 material.

In the present work, we report a reliable facile method for synthesis of SnO_2 -carbon composites, wherein ultrafine SnO_2 particles are filled inside meso-pores of modified ordered mesoporous carbon (denoted as HCMK3), using an incipient wetness technique. In the unique architecture, HCMK3 carbon works as nanocages to confine the SnO_2 nanoparticles inside. During repetitive charge-discharge process, the volume change of SnO_2 occurs continuously, but merely inside the pore space of HCMK3 framework while change in total volume of obtained composite is negligible. As a result, the pulverization phenomenon of SnO_2 material is almost totally prevented. Accordingly, the obtained $\text{SnO}_2/\text{HCMK3}$ exhibits the superior electrochemical performance involving cyclability and rate capability.

2. Experimental

2.1 Synthesis of CMK3

Ordered mesoporous carbons (CMK3) were prepared by a nano-casting method using the hard templates of SBA-15, which was synthesized as previously reported process [7, 8], and sucrose as a source of carbon [8]. In particular, 4 g of SBA-15 was dispersed in an aqueous solution containing 5 g of sucrose and 0.56 g H_2SO_4 for 1 h in an ultrasonic bath. Next, the mixture was dried in an oven until its turned to the dark brown color, then ground into the powder. The fine powder was re-dispersed in 20 mL of another aqueous solution containing sucrose (3.2 g) and H_2SO_4 (0.36 g) and followed by a drying process at 100 °C for 12 h. Subsequently, SBA-15

* Corresponding author: Tel.: (+84) 973.469.466
Email: hang.lethithu@hust.edu.vn

filled by sucrose was carbonized at 900 °C for 5 h in an argon atmosphere to generate the SBA-15/CMK3 composite. To remove the SBA-15 silica template, SBA-15/CMK3 composite was soaked in 5 wt% HF solution for 8 h. Finally, CMK3 product was centrifuged, washed, and dried at 100 °C under vacuum overnight.

2.2 Synthesis of SnO₂/HCMK3 composite

The composite was prepared via incipient wetness impregnation technique of SnCl₄ and followed by chemical reduction of NaBH₄. To enhance surface wettability, CMK3 was oxidized in 2M HNO₃ solution at 80 °C for 1 h under magnetic stirring [9]. After oxidation, the sample was recovered, washed thoroughly, dried and denoted as HCMK3. After that, 1 g of HCMK3 was dispersed ultrasonically into 5 mL of a solution of SnCl₄.5H₂O (32 wt%) in a closed vial for 2 h. A mixture of HCMK3 and SnCl₄ was then dried at 50 °C overnight. After complete drying, the mixture of SnCl₄/HCMK3 was mixed with NaBH₄ powder and exposed in the air for 48 h. The weight ratio of SnCl₄/HCMK3 to NaBH₄ was 1:3. In the next step, the product was washed thoroughly, and dried at 100 °C. The impregnation process was repeated several times to increase SnO₂ loading mass.

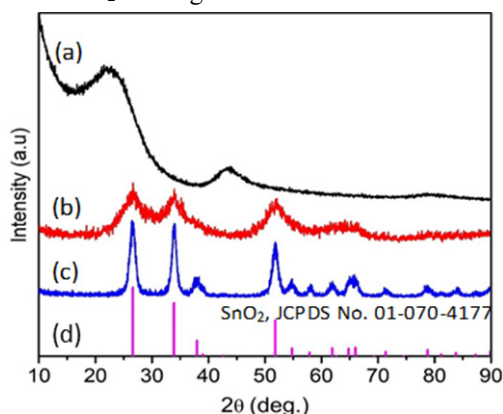


Fig. 1 - X-ray diffraction patterns of (a) HCMK3, (b) SnO₂/HCMK3, (c) pure SnO₂ and (d) SnO₂ reference from JCPDS database

For comparison, nanosized-pure SnO₂ was also prepared by hydrothermal method. Particularly, a mixture of SnCl₄.5H₂O (4.2 g) and Na₃C₆H₅O₇ (8.82 g) was dissolved in 30 mL of deionized water. In addition to it, 30 mL of a solution of 0.24 g NaOH was dropped under magnetic stirring for 10 min, then transferred into a Teflon-lined autoclave and heated at 180 °C for 12 h. The resultant precipitate was collected and rinsed until the supernate was free of chloride ions.

2.3 Material characterization

The microstructure and physicochemical properties of materials were characterized using a high-resolution X-ray diffractometer (XRD, D/MAX Ultima III, Rigaku, Japan), a scanning electron microscope (SEM, S-4700/EX-200, Hitachi, Japan), a high resolution transmission electron microscope (HR-TEM, Tecnai G2, Philips, the Netherlands), a X-ray photoelectron spectroscopy instrument (XPS, Multilab 2000, VG, UK), a thermogravimetric analyser (TGA, TGA-50, Shimadzu, Japan), and Brunauer-Emmett-Teller (BET) analysis (ASAP 2020, Micromeritics, USA).

2.4 Electrochemical characterization

Electrochemical experiments were implemented using coin type cells (CR 2032 type). The SnO₂/HCMK3 electrode was prepared by casting method. A mixture of SnO₂/HCMK3 as electrode active material, super P carbon as conductive agent, and lithium polyacrylate as binder at a weight ratio of 8:1:1 was well mixed in an adequate amount of deionized water and then casted on a Cu foil current collector using a doctor blade. After drying in a into 14 mm diameter disks. Coin half-cells of a SnO₂/HCMK3 electrode as working electrode, a Li electrode as counter and reference electrodes and a glass fiber separator (Whatman) soaked in 80 μL of the electrolyte of 1 M LiPF₆ in ethylene carbonate (EC), dimethyl carbonate (DMC) (EC/DMC = 1v:1v), and 5 wt% fluoride ethylene carbonate additive (FEC), were assembled in the glovebox.

Cyclic voltammogram (CV) measurements were carried out using Gamry PC750 potentiostat. The cells were discharged and charged at the potential range of 0.01-1.5 V vs. Li/Li⁺ using an automatic battery cycler (WonATech-WBCS 3000). The specific capacity was calculated based on the mass of the active materials only.

3. Results and discussion

3.1 Physicochemical characterization

Fig.1 presents XRD patterns of HCMK3, SnO₂/HCMK3 and SnO₂. In Fig.1a, only two peaks of HCMK3 were found at $2\theta = 22.4^\circ$ and 43.2° , corresponding to the (002) and (100) diffractions due to graphitic structure [10]. This implies the presence of a small amount of stacked crystalline graphite phase in HCMK3. Meanwhile, the XRD pattern of SnO₂/HCMK3 presents four broad peaks (Fig.1b). These reflection peaks match well with the standard XRD pattern of SnO₂ (JCPDS, No. 01-070-4177), indicating the tetragonal structure of SnO₂ in the synthesized composite. It is noted that all peaks of SnO₂/HCMK3 are broad, indicating the nano-sized crystallite nature. In addition, no peaks of HCMK3 are observed. This is attributed to (i) the covering of

SnO₂ on the surface of HCMK3 (indicated by SEM images below), (ii) weak reflection intensity of HCMK3 caused by low crystallinity degree, and (iii) the low content of HCMK3 in SnO₂/HCMK3 composite (confirmed by TGA result). In contrast, the

hydrothermally synthesized SnO₂ shows the sharp reflection peaks although its pattern is indexed the same phase with that of the SnO₂/HCMK3 composite (Fig.1c). No impurity phase was detected for both SnO₂ and SnO₂/HCMK3.

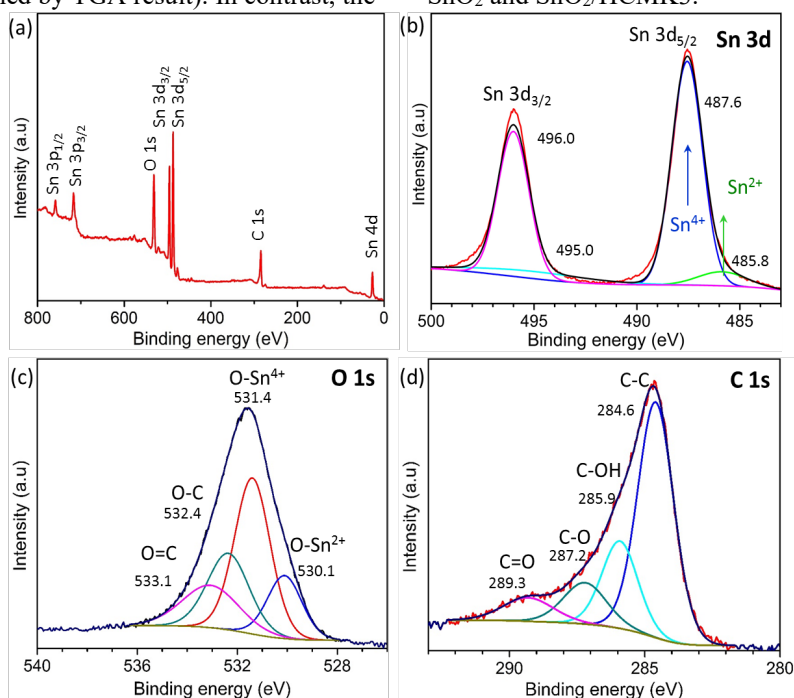


Fig. 2 – (a) XPS full spectrum, (b) the deconvoluted Sn 3d, (c) O1s, and (d) C1s spectra of the SnO₂/HCMK3.

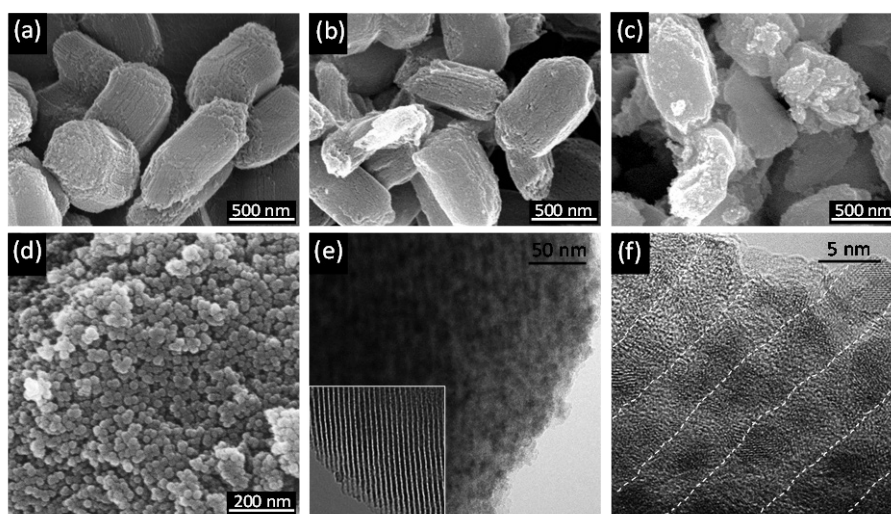


Fig. 3 - SEM images of (a) SBA-15, (b) HCMK3, (c) SnO₂/HCMK3, (d) pure SnO₂; (e, f) TEM images at low and high magnifications of SnO₂/HCMK3. Inset in (e) is TEM image of HCMK3.

Fig.3a-d show SEM images of the obtained samples. The micrograph shows that the morphology of three samples, SBA-15 (Fig.3a), HCMK3 (Fig.3b), and SnO₂/HCMK3 (Fig.3c) is almost the same. They were composed of uniform nanorods with a length of ~800 nm. As an exact replica of the SBA-15

templates, the HCMK3 showed the rough surface after removal of the templates by HF etching process.

Meanwhile, the surface of the SnO₂/HCMK3 nanorods became smoother. This is due to filling SnO₂ inside the pores of HCMK3. However, the SnO₂/HCMK3 nanorods appear to gather together,

suggesting the presence of a part of SnO₂ outside the HCMK3 nanorods when the content of SnO₂ in the composite sample was relatively high, about 61.2 wt.%, which was determined from TGA analysis.

To further identify successful impregnation of SnO₂ in HCMK3, TEM analysis was performed. It is easy to see that in comparison with the HCMK3 sample (inset in Fig.3e), apart from the ordered parallel channels of carbon matrix, a vast number of black spots distributing evenly in the entire nanorod was recognized for the SnO₂/HCMK3 sample (Fig.3e). Especially, in a high-magnification TEM image (Fig.3f), the ~3 nm-SnO₂ nanoparticles seem to be arranged in necklace-like chains, which is like the orientation of the mesoporous channels of carbon matrix in HCMK3. Thus, the uniformly sized SnO₂ nanoparticles were embedded inside the HCMK3 framework without bulk aggregation of nanoparticles occurring on the outer surface. This finding is contrary to the pure SnO₂ sample obtained from hydrothermal synthesis method (Fig.3d). Thank to harsh synthesis conditions such as high temperature and high pressure, the synthesized pure SnO₂ was composed of 20 nm-nanoparticles. Unfortunately, these particles were agglomerated together.

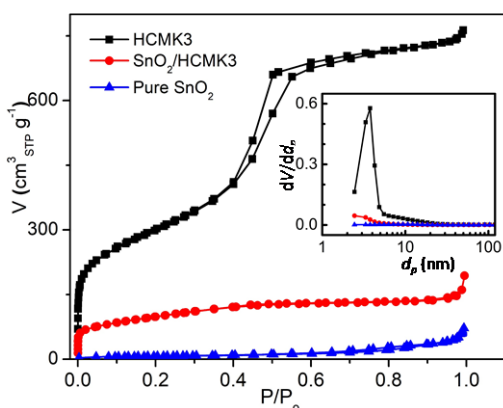
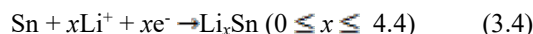
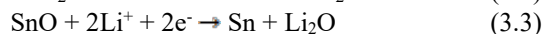


Fig. 4 - N₂ adsorption/desorption isotherms and pore size distribution (inset) of HCMK3, SnO₂/HCMK3 and pure SnO₂.

Fig.4 displays nitrogen sorption isotherms of the HCMK3, SnO₂/HCMK3 and pure SnO₂ samples. Obviously, the typical type with hysteresis loop of mesoporous materials was recorded for HCMK3, but not for SnO₂/HCMK3 and pure SnO₂. The BET specific surface areas of HCMK3, SnO₂/HCMK3 and pure SnO₂ were 1059.9, 346.9 and 25.0 m² g⁻¹, corresponding to the mean pore sizes of 4.4, 3.0 and 15.6 nm, respectively. Thus, the surface area and pore size of HCMK3 reduced dramatically after being filled by SnO₂ nanoparticles. The specific surface area of the SnO₂/HCMK3 was still nearly fourteen times higher than that of the pure SnO₂, suggesting better physical contact with electrolytes in LIBs.

To investigate lithiation/delithiation mechanism of the SnO₂/HCMK3, the half-coin cell using the SnO₂/HCMK3 electrode as working electrode was examined by CV method. Fig.5 shows CV curves of the pure SnO₂ and SnO₂/HCMK3 electrodes for the first three cycles at a scan rate of 0.05 mVs⁻¹ between 0.01 and 1.5 V vs. Li/Li⁺ and open circuit potential as initial potential for the measurements. For the pure SnO₂ electrode, in the first cathodic scan, five peaks were recorded at 2.84, 1.24, 0.87, 0.5 and 0.08 V (Fig.5a). According to the previous reports, lithiation of Sn occurred at a potential below 0.9 V at high temperature and below 0.7 V at room temperature [13, 14]. Thus, the peak at 2.84 V can be assigned to the decomposition of the electrolyte and formation of a solid electrolyte interface (SEI) on the surface of the pure SnO₂. The peaks at 1.24 V and 0.87 V can be attributed to the reduction of SnO₂ to SnO, then to form Sn and Li₂O [15, 16]. The peaks at 0.5 V and 0.08 V corresponds to the formation of a Li-poor and Li-rich series of Li_xSn alloys. All reactions can be expressed as follows:



For the first anodic scan, only two peaks located at 0.59 V and 1.2 V were found. The peaks were related to a de-alloying process of Li_xSn and a redox reaction between Sn and Li₂O to form SnO.

Similarly, for the first cathodic scan, the SnO₂/HCMK3 electrode also shows five peaks, but their position shifts slightly (Fig.5b). This probably stems from the structural difference between the SnO₂/HCMK3 and the pure SnO₂. In addition, two tiny peaks (denoted as C and C') also appear in CV plots of the SnO₂/HCMK3 electrode. The C and C' peaks are associated to lithiation and de-lithiation process of HCMK3 (inset in Fig.5b) [15]. Remarkably, the relative intensity of the anodic peak at 1.18 V of the SnO₂/HCMK3 electrode is higher than that of the pure SnO₂ electrode. This manifests that the presence of HCMK3 in the composite electrode promoted the more reversible redox reaction of Sn to SnO. Hence, the SnO₂/HCMK3 electrode is expected to delivery more capacity.

Compared with the first CV scan, the subsequent CV plots only exhibit two cathodic peaks for both of SnO₂ and SnO₂/HCMK3 electrodes. The position of the peaks hardly shifts. The disappearing cathodic peaks are related to formation of SEI layer, Li-poor Li_xSn alloy and reduction of SnO₂ to SnO. Their disappearance can be explained as follows:

The potential window for CV measurements is from 0.01 V to 1.5 V vs. Li/Li⁺ and open circuit voltage of the cell as starting potential point. Within this potential window, for anodic scanning direction, the oxidation peak related to conversion of SnO to SnO₂ does not appear at all. Therefore, in the end stage of the anodic plot, the active material will be SnO, but not SnO₂. In the subsequent cathodic scanning, there is not the reduction peak corresponding to conversion from SnO₂ to SnO.

In addition, within the window of 0.01-1.5 V for the anodic branch of the CV plot of the first cycle the oxidation peak corresponding to de-formation of SEI layer does not appear and the SEI layer formed previously is still stable. Accordingly, in the next

cathodic scanning, formation of the new SEI layer is insufficient, accompanied by no relevant peak. In fact, the formation of the SEI layer often only occurs in the first cycle. However, it can also happen in the subsequent cycles if the previously formed SEI layer decays due to huge volume change of the electrode active material during long-term cycling process.

Finally, because of undergoing the alloying and de-alloying process at the first cycle as activation process, from the second cycle on, it is possible that the lithiation process occurs more easily. As a result, the peak corresponding to the formation of Li-poor Li_xSn alloy disappears totally for the pure SnO₂ electrode and disappears gradually for the SnO₂/HCMK3 electrode.

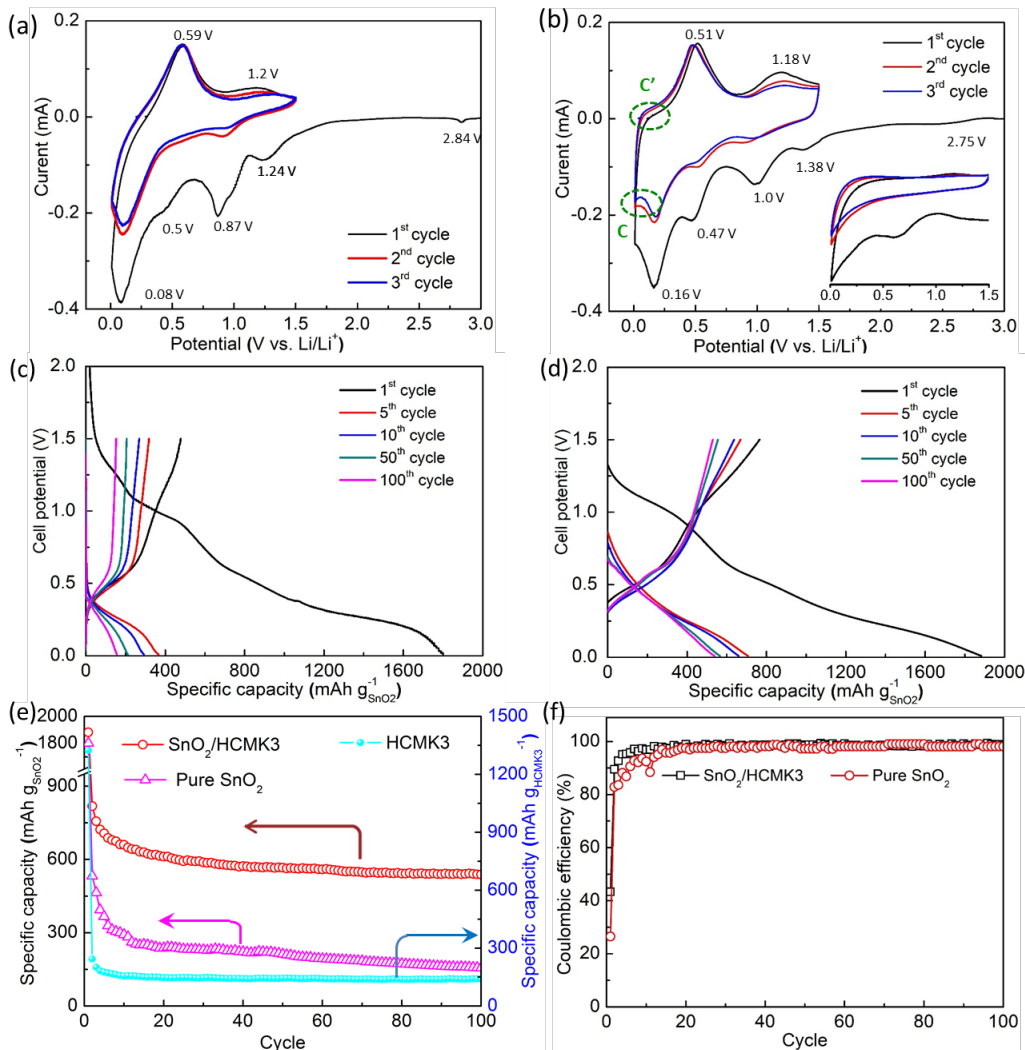


Fig. 5 – (a) Cyclic voltammograms and (c) discharge-charge potential profiles of pure SnO₂. (b) Cyclic voltammograms and (d) discharge-charge potential profiles of SnO₂/HCMK3. (e) The cyclability (discharge) at 0.1C-rate and (f) corresponding coulombic efficiency for 100 cycles.

Fig.5c,d depict the typical discharge and charge voltage profile of the pure SnO₂ and the SnO₂/HCMK3 at 0.1C-rate in the potential range of 0.01-1.5 V. In the first discharge, both electrodes delivered a capacity of about 1800 mAh g⁻¹. However, in the first charge the pure SnO₂ only had a capacity of 477.7 mAh g⁻¹ and the SnO₂/HCMK3 had a capacity of 765.6 mAh g⁻¹. Accordingly, the irreversible capacity in the first cycle of the electrodes was large, viz. 1322.3 mAh g⁻¹ for the pure SnO₂ and 1034.4 mAh g⁻¹ for the SnO₂/HCMK3. This results from the inferior reversibility of the conversion reactions and the irreversible consumption of the active materials. Moreover, because of the high surface area of the electrode active material, amount of the irreversible consumption of the active materials was relatively large.

Theoretically, the SnO₂ can deliver maximum capacity of 1492 mAh g⁻¹ including intercalation and conversion reactions (see reactions (3.2)-(3.4)). Herein, for the first discharge both electrodes show higher capacity than the theoretical value, demonstrating contribution of the side reaction of lithium consumption to form an irreversible product. Furthermore, the initial reversible capacity of the SnO₂/HCMK3 almost reached the theoretical capacity of SnO₂, 782 mAhg⁻¹, which was approximately 97.9% of its theoretical capacity, whilst the pure SnO₂ only achieved about 61.1%. This results from confinement of the SnO₂ nanoparticles in the pores of HCMK3. Since the SnO₂ nanoparticles of the composite did not get agglomerated, most entire the SnO₂ active material completely participated in the lithiation/delithiation process. Consequently, the active material utilization efficiency of the SnO₂/HCMK3 was improved considerably. For the subsequent cycles, the charge-discharge voltage profiles of both electrodes shifted toward low capacity values. However, the pure SnO₂ showed the larger shift than the SnO₂/HCMK3, suggesting the rapid decrease in the reversible capacity during cycling. Besides, the charge and discharge voltage profiles of the SnO₂/HCMK3 electrode almost coincided in the potential range of 0 – 1.0 V, implying the high reversibility of the lithiation/delithiation reaction. Most capacity fading of the SnO₂/HCMK3 in the potential range of 1.0-1.5 V was caused by diminution in reversibility of re-oxidation reaction.

Fig.5e reveals cyclability of the pure SnO₂ and the SnO₂/HCMK3 over 100 cycles at 0.1C-rate. To evaluate the contribution of HCMK3 to the capacity of the SnO₂/HCMK3, a HCMK3 electrode was prepared. As shown in Fig.5e, the discharge capacity of the HCMK3 was small, about 140 mAh g⁻¹. Thereby, when accounting for per 1 g of

SnO₂/HCMK3 composite the contribution of HCMK3 was 54.3 mAh to the actual capacity of SnO₂/HCMK3. This value seems to be relatively low. Meanwhile, distribution of SnO₂ was found to be large. In detail, during the cycling process the capacity of the SnO₂/HCMK3 electrode fluctuated around 577 mAh g⁻¹ accounted for SnO₂ distribution.

In general, the capacity of the SnO₂/HCMK3 electrode almost doubled that of the pure SnO₂ electrode during the discharge-charge process. After 100 cycles, the SnO₂/HCMK3 still delivered a reversible capacity of 529.7 mAh g⁻¹, corresponding to a capacity loss of 0.31% per cycle. It is indicative of high stability of the SnO₂/HCMK3 electrode. In contrast, the pure SnO₂ only delivered a capacity of 153 mAh g⁻¹ after 100 cycles with the capacity loss of 0.68% per cycle. Further, based on coulombic efficiency in Fig.5f it can be also concluded that deposition of majority of SnO₂ nanoparticles in the pores, as well as partial deposition of SnO₂ nanoparticles onto HCMK3 improved the coulombic efficiency significantly. In the first cycle, the pure SnO₂ suffered a quite low coulombic efficiency of 26.5%. This is ascribed to irreversible decomposition reaction of SnO₂ when the upper cut-off voltage was limited at 1.5 V. As the SnO₂ nanoparticles were confined inside as well as covered on the carbon matrix of the HCMK3, the coulombic efficiency was enhanced up to 43.4%. The initial coulombic efficiency strongly impacts in the capacity of the subsequent cycles. Therefore, the higher initial coulombic efficiency of the SnO₂/HCMK3 is among signals indicating the better electrochemical performance. From the second cycle onwards, the coulombic efficiency of both electrodes increased significantly. After 20 cycles, the coulombic efficiency was over 97% for the pure SnO₂ and approximate 99% for the SnO₂/HCMK3.

To prove the excellent rate capability of the SnO₂/HCMK3 electrode, the cells were cycled at various charge-discharge rates from C/10 to 20C for each five cycles. From Fig.6a, it is observed that the rate capability of the SnO₂/HCMK3 was improved, especially at high C-rates. At the high C-rates of 5C, 10C, and 20C, the SnO₂/HCMK3 delivered a reversible capacity of 476, 398.5 and 286.8 mAh g⁻¹, respectively. Unfortunately, at such high C-rates, the pure SnO₂ only delivered a reversible capacity of 70.8, 11.3 and 1.4 mAh g⁻¹, respectively. It demonstrates that the pure SnO₂ electrode hardly works at high drain currents. When the rate of charge-discharge was returned to the initial value of C/10, the pure SnO₂ only recovered a capacity of 222.5 mAh g⁻¹ while the SnO₂/HCMK3 could recovery up to 500 mAh g⁻¹.

Besides, the electrodes were also examined at 1C-rate for 500 cycles. Prior to cycling test, the cells were cycled at 0.1C-rate in the five cycles for activation. As shown in Fig.6b, after 500 cycles the SnO₂/HCMK3 could deliver a capacity of 398.6 mAhg⁻¹, even higher than that of commercial graphite anode, corresponding to a retention of 77.5% of its maximum capacity achieved during cycling. Meanwhile, the pure SnO₂ only remained a low reversible capacity of 44.5 mAh g⁻¹, corresponding to 35.9% of the highest capacity that it could achieved at this rate. Remarkably, despite being activated for 5 cycles at the low rate of charge and discharge, both electrodes only reached their maximum reversible capacity after around 20 cycles of operation. This implies that under a harsh charge-discharge condition the longer activation process for the cells is necessary. Herein, the excellent cyclability of the SnO₂/HCMK3 at such a high rate was arisen from synergistic effect of ultrafine SnO₂ particles

incorporating with the firmly porous matrix of HCMK3. As the size of SnO₂ particles decreases to several nanometers, the ultrafine SnO₂ particles inevitably suffer the huge volume expansion caused by lithiation. Therefore, with the normal structures of carbon, for example amorphous carbon coating [5], graphene [17], and carbon nanotubes (CNTs) [18], the SnO₂ particles obtained after preparation solely anchoring on the carbon materials are easily detached from them after a certain short period of cycling. However, owing to the porous 3D structure of HCMK3 and good electrical conductivity, the HCMK3 became a stable framework supporting for the ultrafine SnO₂ particles. The HCMK3 also played a role as buffer layer and had enough void space to accommodate the volume expansion of SnO₂ during lithiation. As a result, the total outside volume of the SnO₂/HCMK3 was preserved during the repetitive cycling process, thus followed by a good capacity maintenance in the SnO₂/HCMK3 electrode.

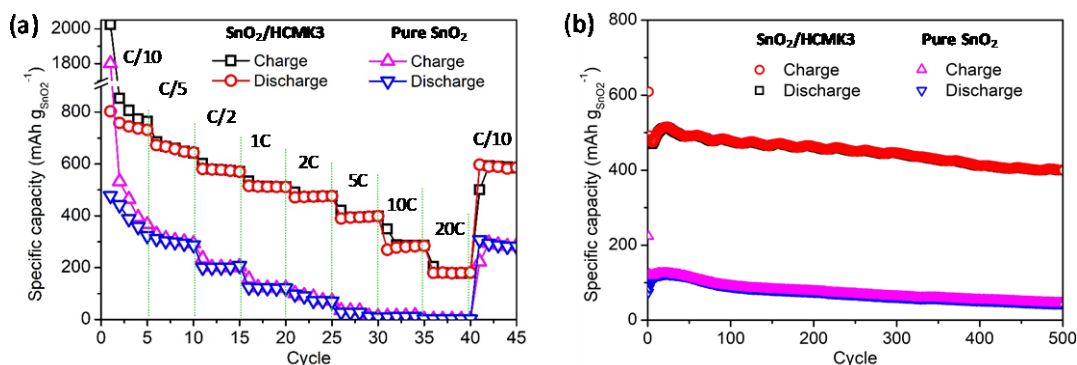


Fig. 6 - (a) Rate capabilities from a charge-discharge rate of C/10 to 20C and (b) cyclability at 1C-rate of the SnO₂/HCMK3 and the pure SnO₂. 1C = 780 mAh g⁻¹.

4. Conclusion

The SnO₂/HCMK3 composite have been synthesized successfully by incipient wetness impregnation and chemical deposition techniques. The obtained SnO₂/HCMK3 composite exhibited the superior electrochemical performance involving high reversible capacity, excellent rate capability and superior long-term cycling performance at the high rate of charge-discharge. From the obtained empirical data, the SnO₂/HCMK3 composite is believed to work as an ultra-stable anode material for lithium ion batteries when its intrinsic electrical properties are improved further through enhancing the electrical conductivity for both SnO₂ and HCMK3. The various strategies such as doping nitrogen in HCMK3, increasing a degree of graphitization for HCMK3, or doping antimony in SnO₂, have been proceeded.

Acknowledgments

This work was granted by Vietnam Ministry of Education and Training (MOET) through the scientific research project (B2018-BKA-62).

References

- [1] C. Wang, G. Du, K. Stähl, H. Huang, Y. Zhong, J.Z. Jiang; Ultrathin SnO₂ Nanosheets: Oriented Attachment Mechanism, Nonstoichiometric Defects, and Enhanced Lithium-Ion Battery Performances; *J. Phys. Chem. C*, 116 (2012) 4000-4011.
- [2] L. Pan, K.-X. Wang, X.-D. Zhu, X.-M. Xie, Y.-T. Liu; Hierarchical assembly of SnO₂ nanowires on MnO₂ nanosheets: a novel 1/2D hybrid architecture for high-capacity, reversible lithium storage; *J. Mater. Chem. A*, 3 (2015) 6477-6483.
- [3] Z. Wang, D. Luan, F.Y.C. Boey, X.W. Lou, Fast Formation of SnO₂ Nanoboxes with Enhanced Lithium Storage Capability; *J. Am. Chem. Soc.*, 133 (2011) 4738-4741.

- [4] L. Li, H. Zhang, Z. Li, W. Zhong, H. Liao, Z. Li; Rapid preparation of SnO₂/C nanospheres by using organotin as building blocks and their application in lithium-ion batteries, *RSC Adv.*, 7 (2017) 34442-34447.
- [5] C. Yong, L. Qian, W. Chunli, S. Lianshan, Y. Zheng, W. Limin; Large-Scale Fabrication of Core-Shell Structured C/SnO₂ Hollow Spheres as Anode Materials with Improved Lithium Storage Performance, *Small*, 13 (2017) 1701993.
- [6] S. Goriparti, E. Miele, F. De Angelis, E. Di Fabrizio, R. Proietti Zaccaria, C. Capiglia; Review on recent progress of nanostructured anode materials for Li-ion batteries; *J. Power Sources*, 257 (2014) 421-443.
- [7] D. Zhao, J. Feng, Q. Huo, N. Melosh, G.H. Fredrickson, B.F. Chmelka, G.D. Stucky, Triblock Copolymer Syntheses of Mesoporous Silica with Periodic 50 to 300 Angstrom Pores, *Science*, 279 (1998) 548.
- [8] X. Ji, K.T. Lee, L.F. Nazar; A highly ordered nanostructured carbon-sulphur cathode for lithium-sulphur batteries, *Nat. Mater.*, 8 (2009) 500.
- [9] P.A. Bazula, A.-H. Lu, J.-J. Nitz, F. Schüth; Surface and pore structure modification of ordered mesoporous carbons via a chemical oxidation approach; *Microporous Mesoporous Mater.*, 108 (2008) 266-275.
- [10] D. Saikia, T.-H. Wang, C.-J. Chou, J. Fang, L.-D. Tsai, H.-M. Kao; A comparative study of ordered mesoporous carbons with different pore structures as anode materials for lithium-ion batteries; *RSC Adv.*, 5 (2015) 42922-42930.
- [11] H. Qiao, J. Li, J. Fu, D. Kumar, Q. Wei, Y. Cai, F. Huang; Sonochemical Synthesis of Ordered SnO₂/CMK-3 Nanocomposites and Their Lithium Storage Properties; *ACS Appl. Mater. Interfaces*, 3 (2011) 3704-3708.
- [12] L. Liu, M. An, P. Yang, J. Zhang; Superior cycle performance and high reversible capacity of SnO₂/graphene composite as an anode material for lithium-ion batteries; *Sci. Rep.*, 5 (2015) 9055.
- [13] I.A. Courtney, J.S. Tse, O. Mao, J. Hafner, J.R. Dahn; Ab initio calculation of the lithium-tin voltage profile; *Phys. Rev. B*, 58 (1998) 15583-15588.
- [14] C.J. Wen, R.A. Huggins; Thermodynamic Study of the Lithium-Tin System; *J. Electrochem. Soc.*, 128 (1981) 1181-1187.
- [15] J. Yang, L. Xi, J. Tang, F. Chen, L. Wu, X. Zhou; Three-dimensional porous carbon network encapsulated SnO₂ quantum dots as anode materials for high-rate lithium ion batteries; *Electrochim. Acta*, 217 (2016) 274-282.
- [16] Y. Dong, Z. Zhao, Z. Wang, Y. Liu, X. Wang, J. Qiu; Dually Fixed SnO₂ Nanoparticles on Graphene Nanosheets by Polyaniline Coating for Superior Lithium Storage; *ACS Appl. Mater. Interfaces*, 7 (2015) 2444-2451.
- [17] Y. Yang, X. Zhao, H.-E. Wang, M. Li, C. Hao, M. Ji, S. Ren, G. Cao; Phosphorized SnO₂/graphene heterostructures for highly reversible lithium-ion storage with enhanced pseudocapacitance; *J. Mater. Chem. A*, 6 (2018) 3479-3487.
- [18] C. Ma, W. Zhang, Y.-S. He, Q. Gong, H. Che, Z.-F. Ma; Carbon coated SnO₂ nanoparticles anchored on CNT as a superior anode material for lithium-ion batteries; *Nanoscale*, 8 (2016) 4121-4126